Correlation in a coherent electron beam

Tetsuji Kodama*
Faculty of Science and Technology, Meijo University, Nagoya 468-8502, Japan

Nobuyuki Osakabe
Central Research Laboratory, Hitachi, Ltd., Tokyo 185-8601, Japan

Akira Tonomura
Central Research Laboratory, Hitachi, Ltd., Saitama 350-0395, Japan

(Received 5 April 2011; published 14 June 2011)

Correlations between successive detections in beams of free electrons are studied with a transmission electron microscope. For incoherent illumination of the detectors, a certain random coincidence probability is observed, indicative for uncorrelated arrival times of the electrons. When the illumination is changed from incoherent to coherent, a reduction of the random coincidence probability is observed, indicative for antibunching in the arrival times of the electrons. However, the amount of reduction is larger than the theoretically expected value calculated from the Pauli principle, forbidding more than one identical fermion to occupy the same quantum state. For a certain coherent illumination of the detectors, where we use magnetic lenses in electron microscopes for magnifications of the coherence length, we find an enhanced coincidence probability, indicative for bunching in the arrival times of the electrons. This originates from correlations in beams of free electrons due to Coulomb interactions.

DOI: 10.1103/PhysRevA.83.063616 PACS number(s): 03.75.−b, 05.30.Fk

I. INTRODUCTION

Quantum interference of two independent, but indistinguishable, particles is increasingly important in various areas of physics. The interference between quantum amplitude for two particles, emitted from two source points, to be detected at two detection points, is a direct result of quantum exchange statistics [1]. Such interference is observed in the coincidence probability, compared to that of statistically independent particles, by computing the time correlation function from the arrival times of the particles. When the two detectors are separated by a distance less than the coherence length, the coincidence probability is enhanced for bosons (bunching), while suppressed for fermions (antibunching), even though they do not interact with each other. This phenomenon for the case of photons, known in astronomy as photon bunching in the light emitted by a chaotic source, was first described by Hanbury-Brown and Twiss in 1956 [2].

Atoms are massive particles and of a much shorter wavelength than light photons. The contrasting bunching and antibunching behavior for the case of atoms was verified in the same apparatus using two different isotopes of helium: ^{3}He (a fermion) and ^{4}He (a boson) by Jeltes *et al.* in 2007 [3]. The results can be attributed to the different quantum statistics of each atomic species.

Electrons are massive fermions, but charged particles. The observation of antibunching behavior for the case of electrons in a free beam is enormously difficult. There are two sources of this difficulty: the low degeneracies (the occupation numbers in phase space) of beams and the Coulomb interaction between the electrons. Advances in field electron emitters with high degeneracies have led to the experimental realizations of observing the antibunching behavior with electrons in a free beam [4]. The antibunching behavior in a beam of free electrons was observed by Kiesel *et al.* in 2002 [5,6]. (The antibunching behavior of electrical current in semiconductor devices was observed in 1998 as a suppression of the shot noise [7,8].) The relative reduction in coincidences was found to be in agreement with theoretical expectations, but a detailed study to verify whether the Coulomb interaction between the electrons do not play any significant role in their experiment [9] has yet to be made. The Coulomb potential, which governs the scattering of one charged particle by another, is so long ranged, but any corresponding investigation to remove this doubt has yet to be conducted.

Therefore, this paper deals with basic experimental and theoretical investigations of the antibunching behavior of electrons in a free beam by considering the direct Coulomb interaction between two individual electrons with the aim of gaining a real understanding of this effect.

II. EXPERIMENTAL RESULTS

A schematic diagram of the experimental setup to observe the antibunching behavior with electrons in a free beam is shown in Fig. 1. The instrument was based on a transmission electron microscope, which has six electromagnetic lenses. Changing the focal length of electromagnetic lenses is done by varying the current through the windings of the electromagnet that makes up the electromagnetic lens. The basic precondition for the appearance of the quantum interference of two electrons was the use of a field emitter, resulting in a high beam degeneracy. The field emitter that we used has a brightness B/E of 5×10^3 A/cm^2 sr eV, an energy full width at half maximum of 0.4 eV, and a coherence time τ_c of 3.9 fs. Electrons were emitted and accelerated to 50–100 keV in the electron

*tkodama@meijo-u.ac.jp

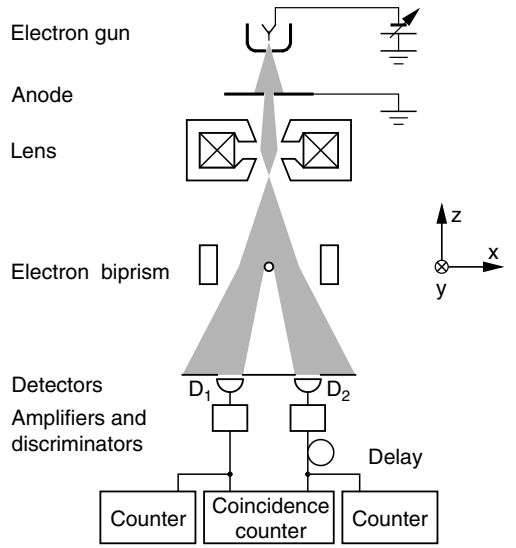

FIG. 1. The experimental setup. The instrument was based on a transmission electron microscope, equipped with six electromagnetic lenses.

gun. Lenses and apertures were set to collimate the electron beam to get various illuminating conditions.

A. The optical system

The focusing action using the two lenses is illustrated in Fig. 2. When the electron beam crosses over at the detectors, the virtual source is in focus, as in Fig. 2(a). As long as the diameter of the beam spot size is smaller than the sensitive area of the detectors, it is not possible to measure the time correlation, so it is necessary to change the focal length of the first lens to defocus the virtual source. This can be seen in the two illustrations in Fig. 2. In Fig. 2(b), little current is passing through the coils of the first lens (EL1) and relatively long focal length occurs, resulting in a large final beam spot size. On the other hand, if the current through the coils of the first lens is increased, it results in shorter focal length and increased final beam spot size [Fig. 2(c)]. The current density j in the electron beam decreases as the final spot size of the electron beam increases.

Usually, the optical systems are used to project a magnified image of the object, a thin specimen, into the plane of the screen. In the experiments, however, there is no specimen in the path of the electrons. Rather, the beam of free electrons is itself an object. This means that the optical system projects the image of a small beam volume into the plane of the screen. The location of the object, the small beam volume, can be varied by changing the focal length of the lenses. The distance between the object and the virtual source is equal to the amount of defocusing Δ which can be calculated by direct application of the lens equation. In this case, the equation for the first lens (EL1) becomes

$$1/a_1 + 1/b_1 = 1/f_1 \tag{1}$$

and that for the second lens (EL2)

$$1/a_2 + 1/b_2 = 1/f_2, \tag{2}$$

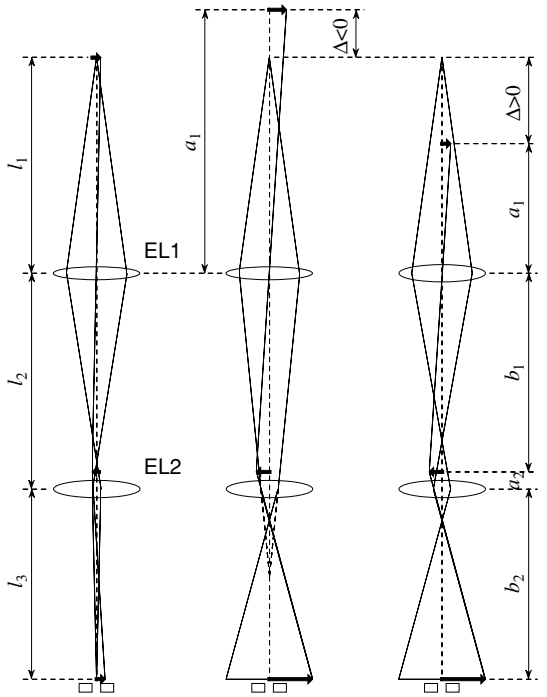

(a) Correct focal length; in focus (b) Long focal length (c) Short focal length

FIG. 2. The focusing action of two lenses. The optical system projects the image of a small beam volume into the plane of the detectors.

where a_i, b_i, and $f_i (i = 1,2)$ are the object, the image distances, and the focal length, respectively. a_2, b_1, and b_2 remain constant as we change f_1 for defocusing the virtual source. Then a_1 depends only on f_1 by Eq. (1). Geometry shows that $\Delta = l_1 - a_1(f_1)$, where l_1 is the distance from the virtual source to the first lens. If the virtual source is focused on the detectors, then $\Delta = 0$. The shorter focal length makes $\Delta > 0$, and $\Delta < 0$ when relatively long focal length occurs.

The length of transversal coherence $l_\perp$ for a quasi-monochromatic and well-collimated electron beam with circular symmetry is given by

$$l_\perp = \hbar/\overline{p}_\parallel \beta, \tag{3}$$

where β is the beam angular divergence subtended at the observation plane and $p_\parallel$ is the longitudinal component of the kinetic momentum of electrons. The averaging of $p_\parallel$ is to be carried out with the (Gaussian) distribution for scalar density. By inserting the relation $B = j/\pi\beta^2$ into Eq. (3), we obtain

$$l_\perp = (\hbar/\overline{p}_\parallel)\sqrt{\pi B/j}. \tag{4}$$

The brightness B is conserved in an optical system of electromagnetic lenses. Therefore, the decrease in the current density by defocusing the virtual source results in an increase in the length of transversal coherence.

For a well-collimated electron beam with circular symmetry, the final spot size of the electron beam is

$$l_d = \alpha|\Delta M|, \tag{5}$$

where α is a limiting aperture angle (see Fig. 2) and $M = b_1b_2/a_1a_2$ is the total magnification of the lens. The final spot size can be used to estimate the current density in the electron beam striking the detectors. As explained previously, the current density determines the length of transversal coherence. If the transmission electron microscope is operated so that there is a high total magnification of the lenses, the same length of transversal coherence would still be obtained as long as the amount of defocusing was small. It should be noted that the length of transversal coherence depends only on the current density, but remains unaffected by the amount of defocusing or the total magnification of the lenses.

An ideal amplitude splitter such as a half mirror in optics is not available in electron optics; hence, an electron biprism [10] needs to be used. The task of electron biprism is to split the coherent electron wave into two partial waves that are still coherent, as shown in Fig. 1. This separation can be made so large that the time correlation of the spatially adjacent regions can be measured without loss of coherence. In Fig. 2 only the electromagnetic lenses are shown, as only the coherence lengths are affected by the lenses.

B. Counting technique

The selection of an appropriate detector and its housing was the first crucial step in achieving good instrumentation of correlation measurements. Avalanche photodiodes have been used successfully in the electron counting mode for correlation measurements [4]. They are selected because of their short dead time, sharp pulse height distribution, and fast response. The avalanche photodiode that we used has a dead time of 480 ps and a timing jitter of 20 ps in timing detection. Good isolation from electrical interference between the two circuits of diodes is essential, as crosstalk, the coupling of energy from one line to another via mutual capacitance, may become a problem. In order that the degree of coherence might be varied at will, the diode was mounted on a horizontal slide which could be transverse normal to the electron beam.

A digital correlator [11] is needed in order process the time correlation function in real time, because the data rate is quite high. The coincidence time window T of 200 ps is determined by the clock frequency, and the average count n in the clock interval should be $n \ll 1$. The digital correlator allows us to construct the normalized correlation function $g^{(2)}(D_1;D_2,\tau) = \overline{n_1 n_2}/\overline{n}_1\overline{n}_2$, where $\overline{n_1 n_2}$ is the average coincidence counts in a preselected time window T with a delay τ and $\overline{n}_i (i = 1,2)$ is the average counts in the time T registered by the detector D_i. Uncorrelated arrival times of the electrons result in a value of 1 for $g^{(2)}(D_1;D_2,\tau)$. A value larger than 1 indicates bunching for $g^{(2)}(D_1;D_2,0)$, while a value less than 1 indicates antibunching for $g^{(2)}(D_1;D_2,0)$. A recent estimation [12] showed that the value of the correlation function at zero delay is expressed as $g^{(2)}(D_1;D_2,0) \sim 1 - A\tau_c/T$, where $A(\leqslant 1)$ is a factor depending on the spatial coherence and the spin polarization. The antibunching signal $A\tau_c/T$ may be detected by accumulating the data to reduce the statistical fluctuations of the measurement. With the practical value of brightness B/E of 5×10^3 A/cm^2 sr eV for extended operation and the coincidence time window T of 200 ps, the antibunching signal $A\tau_c/T$ was found to be 1.6×10^{-5} and we estimated a data acquisition time of 200 h for detection with a signal-to-noise ratio of 3 [13].

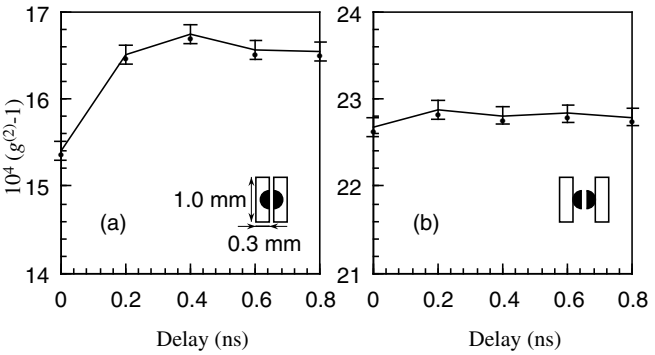

FIG. 3. Normalized correlation functions for (a) partially coherent and (b) incoherent illumination.

C. Not magnified by lenses

The correlation functions $g^{(2)}(D_1;D_2,\tau)$ as a function of the delay τ in the case where no current is passing through the coils of the electromagnetic lenses are shown in Fig. 3. The data acquisition took several hours. The field-emitted current has a tendency to drift slowly, the average counts $\overline{n}_i$ also drift during the measurement time, resulting in a distorted $g^{(2)}(D_1;D_2,\tau)$. We made a number of shorter time-interval measurements and computed the average of the correlation function based on data in each subinterval. The subinterval of 100 s that we used was not sufficiently short compared to flicker noise observed over the frequency 10^2 to 10^5 Hz, which can be related to stochastic process due to surface diffusion and desorption of an adsorbate. Therefore, $g^{(2)}(D_1;D_2,\tau)$ that we observed suffered from an almost constant background, which can be computed from measurements of $g^{(2)}(D_1;D_2,\tau)$ at large values of τ. However, the measured time correlation function, neglecting the baseline, gives a $g^{(2)}(D_1;D_2,\tau)$ curve from $g^{(2)}(D_1;D_2,0)$ to $g^{(2)}(D_1;D_2,0.8\text{ ns})$ with sufficient precision.

In the insets the rectangles represent the sensitive areas of the detectors, the semicircles the coherently illuminated areas split by the electron biprism. The length of transversal coherence $l_\perp$ is 0.22 mm. The initial observations were taken with the sensitive areas effectively adjacent and the result is reported in Fig. 3(a). In this case a small dip was observed in the correlation around zero delay. The small dip completely disappeared, as expected, when the separation of the sensitive areas was large [see Fig. 3(b)], in which position the theoretical correlation is virtually zero. The results shown in Fig. 3 confirm that antibunching is observed when parts of the detectors are coherently illuminated but not when they are widely separated. However, the observed value of the antibunching signal in the data shown is 1.1×10^{-4}, which is one order of magnitude larger than that predicted theoretically from the Pauli principle.

D. Magnified by lenses

When the lengths of transversal coherence $l_\perp$ are increased for totally coherent illumination, the theoretical value of the antibunching signal $A\tau_c/T$ increases in a manner dependent upon the dimensionless parameters, $a_x/l_\perp$ and $a_y/l_\perp$ where

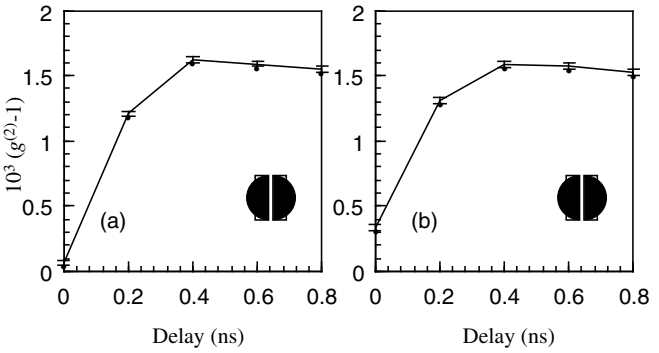

FIG. 4. Effect of an increase in the length of transversal coherence by (a) long and (b) short focal length.

a_x, a_y are the dimensions of the sensitive area along the x, y directions [13]. Figure 4 shows normalized correlation functions $g^{(2)}(D_1; D_2, \tau)$ in the case where the transmission electron microscope is operated so that the lengths of transversal coherence $l_\perp$ are increased to be 0.47 mm. In Fig. 4(a), the focal length of EL1 is relatively long ($\Delta < 0$). On the other hand, in Fig. 4(b), the focal length of EL1 is relatively short ($\Delta > 0$). The absolute values of Δ are calculated to be of the order of 1×10^{-2} m. The value of the antibunching signal is expected to be a few times larger than that for partially coherent illumination. However, the observed values in both cases shown in Fig. 4 are of the order of 1×10^{-3}, that is, one order of magnitude larger than that of Fig. 3(a).

At first sight, if this discrepancy is real, the reader may worry that systematic errors are present in our estimate of the correlations. However, it is shown below that, with a high total magnification of the lenses, we find an enhanced coincidence probability, indicative for bunching in the arrival times of the electrons. The lengths of transversal coherence $l_\perp$ are 0.32 and 0.36 mm for Figs. 5(a) and 5(b), respectively. Owing to the high total magnification, the absolute values of Δ are calculated to be of the order of 7×10^{-4} m, which is one order of magnitude smaller than that of Fig. 4. In the case of Fig. 5(a), where $\Delta < 0$, a reduction of the coincidence probability is still observed. Whereas if $\Delta > 0$, we can obtain an enhanced coincidence probability, as shown in Fig. 5(b). The second important case occurs when a greatly magnified image within a small distance Δ of the virtual source is projected on the

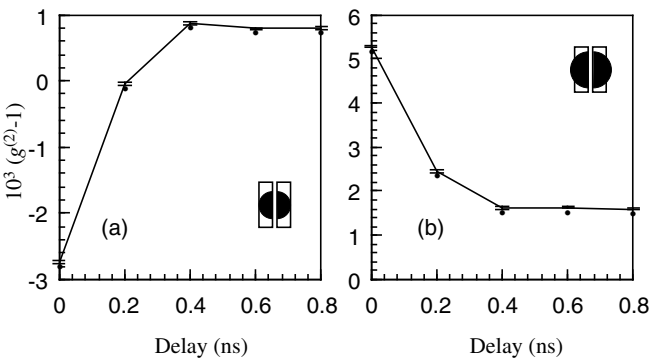

FIG. 5. Effect of an increase in the total magnification of the lenses by (a) long and (b) short focal length.

detectors. In both cases we clearly observe greater correlations of the order of 4×10^{-3}, inconsistent with the theoretically expected values calculated from the Pauli principle. We should also note that the focal lengths can be varied from $\Delta < 0$ to $\Delta > 0$ by quite small changes in the current through an electromagnetic lens. This experiment shows beyond question that the electrons in coherent beams are correlated and that this correlation may originate from the direct Coulomb interaction between two individual electrons.

III. THERMODYNAMIC CONSIDERATIONS

The mutual Coulomb repulsion of the electrons within the beam is the basic process underlying the (energetic) Boersch effect: the broadening of the energy distribution of electron beams at high current densities [14]. The Boersch effect in an optical system is primarily generated by particle interactions in the crossover regions of the beam. This effect has been studied frequently and is now well confirmed experimentally. In addition, it was pointed out by Rose and Spehr that, owing to the Pauli principle, a significant reduction of the Boersch effect is achievable in coherent polarized electron beams.

On the other hand, we are interested in formulas for the correlations between successive detections in beams of electrons. Unlike the Boersch effect, the time correlations are, in fact, insensitive to variations in the geometry of a beam with crossovers. Although the following discussion is based on that of Rose and Spehr [14], we have tried to generalize the theory to the interpretation of the time correlations in coherent electron beams.

The time correlations result from statistical electron-electron interactions within a beam. Here we investigate the average properties of the beam electrons in a small beam volume,

$$V = V_\parallel V_\perp, \tag{6}$$

which moves with the beam and contains N electrons (see Fig. 6). The one-dimensional volume $V_\parallel$ expands when the electrons are accelerated. The two-dimensional volume $V_\perp$ expands in the divergent region and shrinks in the convergent region of the beam. The expansions or compressions of the

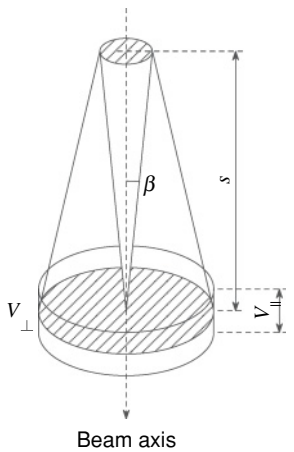

FIG. 6. Geometry of a rotationally symmetric beam.

volumes $V_\parallel$ and $V_\perp$ are assumed to be adiabatic along the beam axis. If the longitudinal motion in a beam is independent of the transverse motion, then the Liouville theorem can be applied to both subspaces separately. Using the Liouville theorem and introducing the longitudinal temperature $T_\parallel$ and the transverse temperature $T_\perp$, one finds the adiabatic relations for a small beam volume:

$$T_\parallel V_\parallel^2 = \text{const}, \qquad T_\perp V_\perp = \text{const}. \tag{7}$$

According to Rose and Spehr the temperatures can be expressed as

$$kT_\parallel = \delta p_\parallel^2/m \tag{8}$$

and

$$kT_\perp = \delta p_\perp^2/m, \tag{9}$$

where $\delta p_\parallel$ and $\delta p_\perp$ denote the corresponding standard deviations of the longitudinal and the transverse momentum components of the electrons and m is the mass of an electron. As we see in the following, the standard deviations of the momentum components are connected with the beam coherence.

A. The longitudinal mode

For a quasi-monochromatic electron beam, the energy deviation δE is small compared with the average kinetic energy of the beam electrons. Then $\delta E_\parallel$ is approximately given by $\delta E \simeq \overline{v}_\parallel \delta p_\parallel$, where $\overline{v}_\parallel$ is the average of the longitudinal velocity component of the electrons [15]. If we assume a beam of totally polarized electrons which consists of a single lateral mode, the Pauli principle requires the inequality $\delta E \tau_c \geqslant \hbar$ where τ_c is the uncertainty in the times at which two electrons cannot be located simultaneously in the time interval t to $t + \tau_c$. Using the inequality together with Eq. (8) and $\delta p_\parallel \simeq \delta E/\overline{v}_\parallel$, we obtain a lower limit for the longitudinal temperature:

$$kT_\parallel = \hbar^2/\overline{v}_\parallel^2 \tau_c^2 m. \tag{10}$$

As was pointed out by Rose and Spehr, the axial distance of two electrons cannot become smaller than the length of longitudinal coherence $\overline{v}_\parallel \tau_c$ resulting from Fermi statistics. Hence, the coherence time τ_c is connected with the lower limit for the longitudinal temperature via Eq. (10).

To examine the behavior of a particle system, one must check which of the effects dominates. Here the effects are correlations due to the Pauli principle and the Coulomb interactions. In Fig. 7(a), the energies $kT_\parallel/2$ of the lower limit for the longitudinal temperature and the corresponding energies $E_c(l_\parallel) = e^2/4\pi\varepsilon_0 l_\parallel$ of each electron in the Coulomb potential at the length of longitudinal coherence $l_\parallel = \overline{v}_\parallel \tau_c$ are plotted on a double logarithmic scale as functions of the coherence time τ_c. To roughly survey the dependence of the energies $kT_\parallel/2$ and E_c on the coherence time τ_c, we consider as an example an electron beam emanating from a field emitter with energy 0.4 eV and accelerated up to 100 kV. These values correspond to average longitudinal velocity components $\overline{v}_\parallel$ of 3.7×10^5 m/s and 1.6×10^8 m/s, respectively. For a coherence time $\tau_c = 1$ fs we obtain from Eq. (10) $kT_\parallel = 0.54$ eV and $E_c = 3.8$ eV at the surface of the cathode. If the electrons are accelerated up to 100 kV, we find $kT_\parallel = 2.8\ \mu$eV and $E_c = 8.8$ meV. In both cases $kT_\parallel/2 < E_c$, so that the dominant mechanism of the correlations must be the direct Coulomb interactions between two individual electrons. With increasing coherence time $\tau_c > 1$ fs the energy $kT_\parallel/2$ of the thermodynamic limit decreases much faster than the energy E_c in the Coulomb potential. Only in the regions $\tau_c < 0.07$ fs at the surface of the cathode and $\tau_c < 0.16 \times 10^{-3}$ fs after the acceleration of the electrons $kT_\parallel/2$ is greater than E_c. Consequently, the Coulomb interactions can be considered as the dominant mechanism of the correlations that we observed.

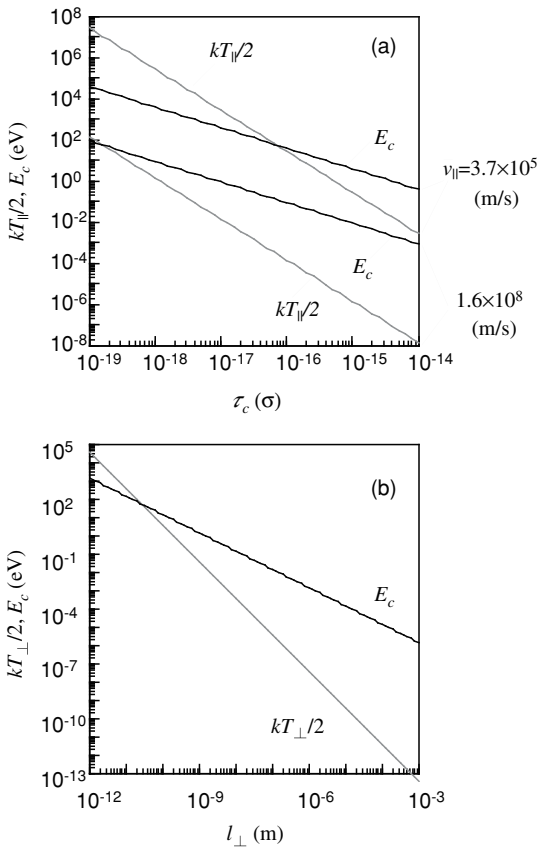

FIG. 7. The energies $kT_\parallel$ and $kT_\perp/2$ obtained by the Pauli principle and the corresponding Coulomb potentials $E_c(l_\parallel)$ and $E_c(l_\perp)$.

B. The transverse mode

For a well-collimated electron beam with circular symmetry, the deviation $\delta p_\perp$ of the transverse momentum component of the electrons is connected with the average $\overline{p}_\parallel$ of longitudinal momentum component by the relation $\delta p_\perp \simeq \overline{p}_\parallel \beta$. By inserting this relation into Eq. (9) and using Eq. (3), we obtain

$$kT_\perp \simeq \overline{p}_\parallel^2 \beta^2/m = \hbar^2/l_\perp^2 m. \tag{11}$$

This relation states that for a beam of a given current $jV_\perp$ the transverse temperature $T_\perp$ is determined by the length of transversal coherence $l_\perp$. It follows from Eq. (7) that the transverse temperatures $T_\perp$ at every focus or crossover can

become very high, since $V_\perp$ is proportional to the cross section of the beam. After passage through the crossover the beam diverges and the transverse temperature $T_\perp$ decreases quadratically with increasing the distance s from the crossover (Fig. 6). This behavior implies that the highest transverse temperature and hence the minimum length of transversal coherence are obtained at the crossover. In Fig. 7(b), the energies $kT_\perp/2$ of the transverse temperature and the corresponding energies $E_c(l_\perp) = e^2/4\pi\varepsilon_0 l_\perp$ of each electron in the Coulomb potential at the length of transversal coherence $l_\perp$ are plotted on a double logarithmic scale as functions of $l_\perp$. For a length of transversal coherence $l_\perp = 0.1$ mm we obtain from Eq. (11) $kT_\perp = 0.008$ neV and $E_c = 0.014$ meV, so that $kT_\perp/2 \ll E_c$. With increasing length of transversal coherence $l_\perp > 0.1$ mm the energy $kT_\perp/2$ of the thermodynamic limit decreases much faster than the energy E_c in the Coulomb potential. Only in the region $l_\perp < 0.03$ nm $kT_\perp/2$ is greater than E_c. In practice the dominant mechanism of the transverse motions must be the Coulomb interactions.

IV. ANALYTICAL CALCULATIONS

A thermodynamic equilibrium of the beam electrons in a small beam volume will be established only if the electrons suffer many collisions in the region between the emitter and the observation plane. This is the case for very high current densities obtained with thermionic cathodes. In the case of low current densities, only few collisions occur. Then it is appropriate to assume that the main contribution to the correlations results from a single scattering which altered the direction of two neighbor electrons. To simplify the discussion, we restrict our investigations to nonrelativistic calculations in the laboratory system. As shown in Fig. 8, we consider two electrons e_1 and e_2 moving in directions parallel to the beam axis. Suppose the initial velocity of e_1 to be $v + \Delta v$, e_2 to be v, and the difference between the initial positions of the two electrons perpendicular to the beam axis is Δx, which implies that an impact parameter of two colliding electrons is equal to Δx. After the collision the electrons are deflected by an angle χ, which is related to the impact parameter Δx and the initial velocity Δv moving in opposite directions in the center of mass frame by

$$\tan(\chi/2) = e^2/2\pi\varepsilon_0 m(\Delta v)^2\Delta x. \tag{12}$$

When referring back to the laboratory system, e_i is scattered by an angle $\theta_i (i = 1,2)$. From Fig. 8, it follows that the angle θ_i is connected with the angle χ and the velocity $v_i (i = 1,2)$ of the two electrons after their encounter by the relation

$$\sin\theta_i = \Delta v \sin\chi/2v_i. \tag{13}$$

If the velocities of any two electrons within their center of mass system are small compared to the mean velocity of the electrons in the laboratory system, then the difference between the initial energies of the two electrons can be expressed as $\Delta E \simeq mv(\Delta v)$. Using the relation for two electrons with ΔE, the maximum angle,

$$\tan\theta_m \simeq \frac{1}{1 + 2mv^2/\Delta E}, \tag{14}$$

is obtained when they are deflected in directions perpendicular to the beam axis in the center-of-mass frame. In this case $\chi = \pi/2$, and the corresponding velocity of the two electrons after their encounter is found as $v_1 = v_2$.

The long-range Coulomb potential will cause a slight deflection no matter how far apart the colliding electrons are from each other. Now we assume that the main contribution to the time correlations results from the collision between the electrons which are deflected by the angles θ_i larger than the beam angular divergence β. Most collisions occur in the region near the tip or focus of the beam, where the electron density is high. However, according to Eq. (14), the amount of large angle scattering will decrease with increasing the velocity v of the two electrons. This restricts the velocity v for a given energy deviation ΔE. For example, if we take $\theta_m = 10^{-4}$, we obtain from Eq. (14) that the maximum velocity of the two electrons for $\Delta E = 0.1$ eV is about 9.4×10^6 m/s, while for $\Delta E = 0.01$ eV the maximum velocity is 3.0×10^6 m/s. As a consequence, we consider that most of the collisions, which cause the time correlations, occur in front of the tip, where the electrons start with initial velocities of 3.7×10^5 m/s and are accelerated up to 1.6×10^8 m/s by a compound system of electrostatic and magnetic lenses.

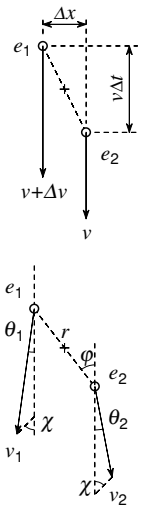

FIG. 8. Two colliding electrons e_1 and e_2 moving in directions parallel to the beam axis.

A. The expected correlation by Coulomb repulsion

To obtain an expected value of the time correlations we assume that the starting times of the different electrons are not correlated. Then the distribution function for time intervals between adjacent starting times t can be expressed as the simple exponential shape $\lambda e^{-\lambda t}$, where λ is the average rate at which electrons are starting. The probability of time intervals smaller than t can be obtained by integrating this distribution between 0 and t:

$$p(t) = \int_0^t \lambda e^{-\lambda t'} dt' = 1 - e^{-\lambda t}. \tag{15}$$

In the experiments, the counting rate is low enough so that $\lambda t \ll 1$. Then Eq. (15) reduces to $p(t) \simeq \lambda t$.

The time necessary for an electron to be accelerated in the electron gun is of the order of 2×10^{-9} s. During this time the electron encounters neighbor electrons with the initial velocity Δv in the center-of-mass frame. In a sufficiently small paraxial domain, the difference of two colliding electrons' positions r can be approximated by the axial distance of the two electrons $l = v\Delta t$. Thermodynamic considerations are useful for determining an expected value of the time correlations by Coulomb scattering. The minimum axial distance l_m of two colliding electrons is obtained from the conservation of energy: $kT_\parallel/2 = E_c(l_m)$ as

$$l_m = e^2/2\pi\varepsilon_0 kT_\parallel. \tag{16}$$

When the electrons are accelerated, the longitudinal temperature $T_\parallel$ is decreased according to Eq. (10), resulting in an increase of l_m. Owing to this behavior, each of the two electrons, which are separated initially by an axial distance $l < l_m$, is scattered by the angles θ_i. If the angles θ_i exceed the beam angular divergence β, the Coulomb scattering will cause a correlation between the arrival times of the electrons which strike the detectors. To obtain an expected value of the correlation function we assume that the characteristic length of the correlations l_c, which is related to the correlation time t_c by $l_c = \overline{v}_\parallel t_c$, is found from Eq. (16) using the maximum velocity given by Eq. (14).

B. The shift of virtual source point

In geometrical optics, we treat light beams as rays that propagate along straight lines except at the lens, where the rays may be bent or refracted. This approach had been also assumed to be completely accurate for beams of free electrons, which propagate along straight lines except at the lens, where the beams may be deflected. However, we recognize that the Coulomb scattering among the electrons within the beam also causes a significant deflection for the electrons within the correlation length. The simple model based on the two electron collision approximation gives us a good description of the trajectory displacement caused by the collisions in front of the tip. If the center of mass of the two electrons moves nearly parallel to the beam axis in the laboratory system, then it will coincide with a point in front of the tip at the time when the difference of two electrons' positions reaches a minimum. As shown in Figs. 9 and 10, trajectories starting from the virtual source A are bent in such a way that their asymptotes intersect in a small zone around the point B, and after the collision the virtual source point of the two electrons will shift from A to B. This implies that in front of the tip, the trajectories of the electrons within the correlation length are bent in such a way that they seem to have emerged from the point B. The effect resulting from a shift of virtual source point for the electrons within the correlation length depends on the path of the electrons through the lenses. We consider that the amount of defocusing Δ will determine the influence of the shift of virtual source point on the correlation between the arrival times of the electrons.

In the case of the short focal length with a high total magnification of the lenses $0 < \Delta \leqslant 7 \times 10^{-4}$ m, the small zone around the virtual source point B can be focused on the detectors. From the classical point of view, this will lead to an enhanced coincidence probability, indicative for bunching in the arrival times of the electrons, because without shifting the virtual source point, parts of the electrons within the correlation length will not strike the detectors, as shown in Fig. 9. Without an analysis based on quantum statistics, it can be expected to exhibit an enhanced coincidence probability, which originate from Coulomb repulsion of the electrons within the beam. To obtain an expected value of the correlation function for this behavior, we assume that the joint probability that the first electron e_2 arrives at the detector D_2 and another electron e_1 arrives at the detector D_1 within the coincidence time window $T(>t_c)$ is proportional to $p'(t_c) = 1 - e^{-\lambda' t_c}$, where λ' is an

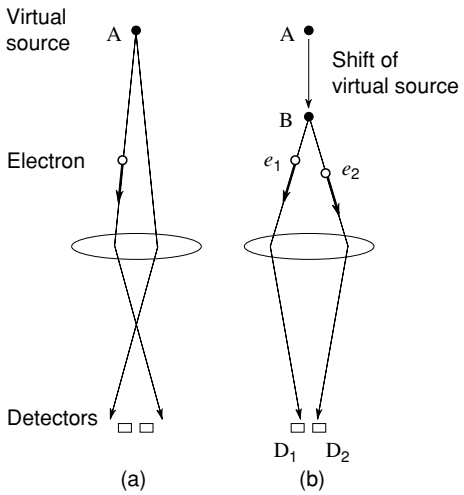

FIG. 9. Influence of the shift of virtual source point from A to B when the point B is focused on the detectors as in Fig. 2(c). (a) Parts of the electrons within the correlation length will not strike the detectors without shifting the virtual source point. (b) The two electrons scattered through large angles by Coulomb potential fall on the detectors within the coincidence time window.

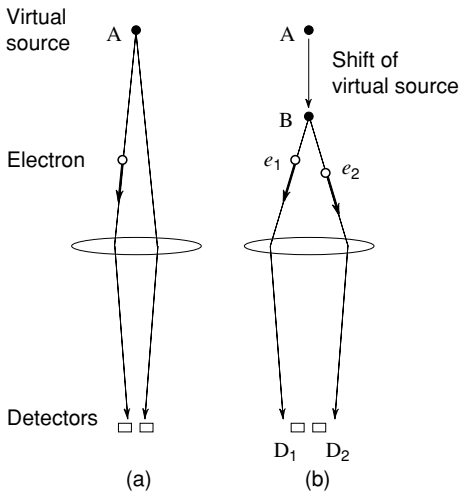

FIG. 10. Influence of the shift of virtual source point from A to B when the point B is not focused on the detectors as in Fig. 2(b). (a) The electrons within the beam will strike the detectors if scattering effects remain negligibly small. (b) The two electrons scattered through large angles by Coulomb potential yield a null probability for joint detection in the coherence area.

average rate depending on the current density near the tip. Then the probability for joint detection in the coherence volume $p(T)$ increases to $p(T) + p'(t_c)/2$. The first term represents the same coincidence probability as the result for a beam of electrons, with an average rate of λ, arranged to fall on the detectors. It includes the process in Fig. 9(b) in which the two electrons scattered through large angles by Coulomb potential fall on the detectors within the coincidence time window. The additional probability represented by the second term arises from the electrons, with an average rate of λ', arranged not to fall on the detectors. For a low counting rate ($\lambda T \ll 1$) the value of the correlation function at zero delay may be written as $g^{(2)}(D_1; D_2, 0) \sim 1 + C\lambda' t_c/2\lambda T$, where $C(\leqslant 1)$ is a factor depending on the energy distribution and the virtual source diameter.

As long as the virtual source point B is not focused on the detectors, the electrons which are scattered by angle $\theta_i > \beta$ yield a null probability for joint detection in the coherence area, as shown in Fig. 10. If t_c is small compared to T, the coincidence probability $p(T)$ decreases to $p(T) - p(t_c)/2$. For a low counting rate ($\lambda T \ll 1$) the value of the correlation function may be written as $g^{(2)}(D_1; D_2, 0) \sim 1 - Ct_c/2T$. This is the case for the long focal length with a high total magnification of the lenses $0 > \Delta \geqslant -7 \times 10^{-4}$ m. On the other hand, blurring the signal and loss of the correlation could be seen in the case of the lower total magnification of the lenses $|\Delta| \geqslant 1 \times 10^{-2}$ m. This is because defocusing the virtual source point B will cause an increase of the process in which electrons initially located out of the coherence area are deflected by the other electrons in the same coherence area. As a result, the value of C depends on the amount of defocusing Δ. When the electromagnetic lenses are not used, the optical system has no crossover. This is equivalent to the case for large amount of defocusing $\Delta \geqslant 1$m. The correlation signal will become smaller, resulting in the minimum value of C.

To survey the dependence of C on the amount of defocusing Δ we have evaluated C numerically for the experimental values of the correlations. A Gaussian distribution and its full width at half maximum $\delta E = 0.4$ eV are assumed for the energy distribution of electron beams. In this case the average energy difference ΔE of two electrons vanishes, because values $\Delta E < 0$ can occur as much probability as values $\Delta E > 0$. For values $\Delta E < 0$ the two electrons move in the same direction in the center of mass frame, so that the Coulomb potential will cause only a slight deflection. Then we choose the average energy difference in the range $\Delta E > 0$ as an appropriate measure of the correlations. This quantity is 0.19 eV for $\delta E = 0.4$ eV. Choosing $\Delta E = 0.19$ eV, $\chi = \pi/2$, and $\theta_m = 10^{-4}$ as an example, one obtains from Eq. (14) the maximum velocity 1.3×10^7 m/s. Inserting this value together with $l_c = \overline{v}_{\parallel} t_c$ into Eq. (16) yields $t_c = 7.4 \times 10^{-12}$ s, which may lead to a theoretical limit for the maximum correlation signal $t_c/2T = 1.84 \times 10^{-2}$ for $T = 200$ ps. In the case of defocusing $\Delta = -0.0007$ m we obtain the value of $C = 0.19$ from the observed value of the correlation signal $g^{(2)} - 1 \simeq g^{(2)}(D_1; D_2, 0) - g^{(2)}(D_1; D_2, 0.8\text{ ns})$. This value seems to be realistic, because the angles χ are distributed at random in the range $0 < \chi < \pi/2$ according to Eq. (12). If the absolute value of defocusing is increased further, the value of C decreases as listed in Table I. The calculations show that the value of C is approximately proportional to $\Delta^{-1/2}$. In the case of defocusing $\Delta = +0.0007$ m we obtain the value of $C\lambda'/\lambda = 0.20$ from the observed value of the correlation signal.

TABLE I. Examples of calculated values.

Defocusing Δ (m)	Experimental value of 10^3 $(g^{(2)} - 1)$	Calculated value of C
−0.01	−1.49 ± 0.03	0.081
−0.0007	−3.52 ± 0.03	0.191
+0.01	−1.20 ± 0.04	0.065
+1.439	−0.11 ± 0.02	0.006

The results obtained with this model are in fairly good agreement with the corresponding experimental values of the correlations. It is now obvious that the Coulomb interactions can be understood as the dominant mechanism of the correlations. An exact determination of the values of parameters would require extensive numerical calculations of the paths of all the electrons in the tip region.

V. CONCLUSIONS

Basic experimental and theoretical investigations of the contrasting bunching and antibunching behavior of electrons in a free beam have been carried out with the aim of a real understanding of this effect. We have developed an analytical treatment of the behavior by considering the direct Coulomb interaction between two individual electrons. In this way, it has proved possible to achieve fairly good agreement with the corresponding experimental values of the correlations. Although the correct determination of the values of parameters is a difficult task, there will be no intrinsic obstacle that renders it impossible.

The antibunching behavior in a beam of free electrons was first described by Kiesel *et al.* [5]. They claimed that the reduction in the probability of the time interval between two successive electron arrivals is due to the Pauli principle. The type of signals they measured differs from the correlation function. However, as was pointed out by Shen [9], the Coulomb interaction appears to be responsible for the effect seen in their experiment. We hope that this investigation provides some new understanding of the physical processes that take place in electron guns.

ACKNOWLEDGMENTS

This work was supported by the "TONOMURA Electron Wavefront" project (1989–1994) of the ERATO program by JST (Japan Science and Technology Agency). We would like to thank T. Urakami, S. Ohsuka, H. Tsuchiya, and Y. Tsuchiya of Hamamatsu Photonics for their invaluable technical collaboration during the setup of the experiment.

[1] G. Baym, *Lectures on Quantum Mechanics* (Addison-Wesley, New York, 1974).
[2] R. Hanbury-Brown and R. Q. Twiss, Nature (London) **177**, 27 (1956).
[3] T. Jeltes *et al.*, Nature (London) **445**, 402 (2007).
[4] N. Osakabe, T. Kodama, J. Endo, A. Tonomura, K. Ohbayashi, T. Urakami, S. Ohsuka, H. Tsuchiya, and Y. Tsuchiya, Nucl. Instrum. Methods Phys. Res., Sect. A **365**, 585 (1995).
[5] H. Kiesel, A. Renz, and F. Hasselbach, Nature (London) **418**, 392 (2002).
[6] F. Hasselbach, Rep. Prog. Phys. **73**, 016101 (2010).
[7] R. C. Liu, B. Odom, Y. Yamamoto, and S. Tarucha, Nature (London) **391**, 263 (1998).
[8] M. Henny, S. Oberholzer, C. Strunk, T. Heinzel, K. Ensslin, M. Holland, and C. Schönenberger, Science **284**, 296 (1999).
[9] K. Shen, Ph.D. thesis, University Illinois, 2009.
[10] G. Möllenstedt and H. Düker, Naturwissenschaften **42**, 41 (1955).
[11] B. Chu, *Laser Light Scattering* (Academic Press, Orlando, 1974).
[12] M. P. Silverman, Phys. Lett. A **120**, 442 (1987).
[13] T. Kodama, N. Osakabe, J. Endo, A. Tonomura, K. Ohbayashi, T. Urakami, S. Ohsuka, H. Tsuchiya, Y. Tsuchiya, and Y. Uchikawa, Phys. Rev. A **57**, 2781 (1998).
[14] H. Rose and R. Spehr, in *Applied Charged Particle Optics*, edited by A. Septier (Academic Press, New York and London, 1983), Vol. C, p. 475.
[15] P. W. Hawkes and E. Kasper, *Principles of Electron Optics* (Academic Press, London, 1996).